HAL
open science

Dual-constellation Vector Tracking algorithm in Ionosphere and Multipath conditions

Enik Shytermeja, Axel Javier Garcia Peña, Olivier Julien

To cite this version:

Enik Shytermeja, Axel Javier Garcia Peña, Olivier Julien. Dual-constellation Vector Tracking algorithm in Ionosphere and Multipath conditions. ITSNT 2017, 4th International Technical Symposium on Navigation and Timing, Nov 2017, Toulouse, France. hal-01759189

HAL Id: hal-01759189

https://enac.hal.science/hal-01759189v1

Submitted on 5 Apr 2018

HAL is a multi-disciplinary open access archive for the deposit and dissemination of scientific research documents, whether they are published or not. The documents may come from teaching and research institutions in France or abroad, or from public or private research centers.

L'archive ouverte pluridisciplinaire **HAL**, est destinée au dépôt et à la diffusion de documents scientifiques de niveau recherche, publiés ou non, émanant des établissements d'enseignement et de recherche français ou étrangers, des laboratoires publics ou privés.

Dual-constellation Vector Tracking algorithm in Ionosphere and Multipath conditions

Enik Shytermeja, Axel Garcia-Pena, Olivier Julien, *ENAC, Toulouse, France*
Email: shytermeja, garcia-pena, ojulien@recherche.enac.fr

BIOGRAPHIES

Enik Shytermeja is a PhD researcher within the SIGnal processing and NAVigation (SIGNAV) research group of the TELECOM lab of ENAC (French Civil Aviation University), in Toulouse, France. He received his master degree in telecommunication engineering in 2011 from the Polytechnic University of Tirana in Albania and his 2nd level master degree in "Navigation and Related Applications" with excellent results in 2012 from Polytechnic University of Turin. His research interests are GNSS signal processing and receiver design, and multipath mitigation in urban environment.

Axel Garcia Pena is a researcher/lecturer with the SIGnal processing and NAVigation (SIGNAV) research group of the TELECOM lab of ENAC (French Civil Aviation University), Toulouse, France. His research interests are GNSS navigation message demodulation, optimization and design, GNSS receiver design and GNSS satellite payload. He received his double engineer degree in 2006 in digital communications from SUPAERO and UPC, and his PhD in 2010 from the Department of Mathematics, Computer Science and Telecommunications of the INPT (Polytechnic National Institute of Toulouse), France.

Olivier Julien is the head of the SIGnal processing and NAVigation (SIGNAV) research group of the TELECOM lab of ENAC (French Civil Aviation University), Toulouse, France. His research interests are GNSS receiver design, GNSS multipath and interference mitigation, and interoperability. He received his engineer degree in 2001 in digital communications from ENAC and his PhD in 2005 from the Department of Geomatics Engineering of the University of Calgary, Canada.

ABSTRACT

In urban environments, standalone GNSS receivers can be strongly affected to the point of not being able to provide a position accuracy suitable for use in vehicular applications. In this paper, a dual constellation GPS + Galileo single frequency L1/E1 Vector Delay Frequency Lock Loop (VDFLL) architecture for the automotive usage in urban environment is presented. In the proposed architecture, the usual scalar tracking loops are abolished and instead an EKF-estimated navigation solution drives the code delay (VDLL part) and carrier frequency (VFLL part) Numerical Control Oscillators (NCOs) in the feedback loop for each tracking channel.

However, the use of single frequency L1 band signals implies the necessity of taking into account the ionospheric error effect. This paper focuses on the implementation of the dual-constellation single-frequency VDFLL architecture, capable of estimating the ionosphere residual error present in the received observations. This work investigates the VDFLL superiority w.r.t the scalar tracking receiver in terms of positioning performance and tracking robustness in urban area in the presence of multipath and ionosphere residual errors. Contrary to the conventional tracking, the L1/E1 VDFLL loop is able to accurately pursue the frequency and code-delay estimation without the requirement of signal reacquisition process and within limited positioning error.

1 INTRODUCTION

In the last decade, Global Navigation Satellites Systems (GNSS) have gained a significant position in the development of positioning and navigation applications and associated services. However, in urban environments, standalone GNSS receiver architectures can be strongly affected to the point of not being able to provide a position accuracy suitable for use in vehicular applications. Two significant signal distortions are generated from the urban environment:

- On one hand, the reception of reflected or diffracted GNSS Line Of Sight (LOS) echoes in addition to the direct LOS signal generates the phenomenon known as multipath. Multipath echoes represent one of the most detrimental positioning error sources in urban canyons. In fact, the reception of echoes distorts the ideal correlation function and leads to a degradation of the signal code and carrier estimations accuracy. Consequently, the pseudo-range and Doppler measurements are degraded.
- On the other hand, the total or partial obstruction of the GNSS LOS by the urban environment obstacles causes GNSS LOS blockage or GNSS LOS shadowing phenomena. The reception of Non-LOS (NLOS) signals due to GNSS LOS signal blockage can then introduce a bias on the pseudo-range measurements if only NLOS satellites are tracked. The LOS shadowing can also decrease the LOS signal C/N_0 and thus makes

International Technical Symposium on Navigation and Timing (ITSNT) 2017
14-17 Nov 2017
ENAC, Toulouse, France

the signal more vulnerable to the multipath effects. Finally, the resulting degraded measurements cause the navigation processor to compute an inaccurate position solution or even to be unable to compute one in the case of few available measurements (few satellites in-view).

Conventional GNSS receivers use a decentralized architecture, separating the signal processing module from the navigation algorithm. In fact, the first block performs the signal acquisition, correlation and tracking tasks for both the code delay and carrier frequency/phase. Whereas, the navigation algorithm that can either employ a Weighted Least Square (WLS) or Kalman filter (KF) technique provides the user's navigation solution and user's clock term estimation. As a result, in scalar tracking configuration in the presence of weak signals or significant signal power drops, loss of lock of the affected satellite tracking loops can occur and therefore, the associated measurements are not passed to the navigation processor due to their lack of accuracy. Therefore, the navigation solution performance can become very poor in urban environments.

A promising approach able to cope with the urban environment-induced effects including multipath, NLOS reception and signal outages is Vector Tracking (VT), which was firstly introduced in [1]. In vector tracking, a deep-integration between the signal processing block and the navigation processor exists since both these tasks are accomplished by the central navigation filter. In comparison to conventional or scalar tracking (ST), where each visible satellite channel is being tracked individually and independently, VT performs a joint signal tracking of all the satellite signals. Vector tracking exploits the knowledge of the estimated receiver's position and velocity to control the receiver's code/carrier tracking feedback. In [1], the Vector Delay Lock Loop (VDLL) architecture is explained in details, for which the navigation filter replaces part of the classical delay lock loops (DLLs) structure with an Extended Kalman filter (EKF). In this configuration, the navigation solution directly drives the code Numerical Control Oscillator (NCOs) of each tracking channel while the carrier frequency/phase estimation is still achieved in a classical scalar way by the Frequency or Phase Lock Loops (FLLs or PLLs). Vector DLL (VDLL) tracking performance of the GPS L1 signal in weak signal-to-noise ratio (SNR) environment and robustness against signal interference and attenuation has been demonstrated in [2], [3] and [4]. Different cascaded vector tracking approaches, associating a local filter per each tracking channel, were examined in [5] and [6].

In this paper, a dual constellation GPS + Galileo single frequency L1/E1 VDFLL architecture in urban environment is presented. This configuration, seen as a combination of the Vectorized DLL (VDLL) and Vectorized FLL (VFLL) loops, represents a concrete application of information fusion, since all the satellite code/carrier tracking channels are jointly tracked and controlled by the common navigation Extended Kalman filter (EKF). In other words, the EKF-estimated navigation solution drives the code delay (VDLL part) and carrier frequency (VFLL part) Numerical Control Oscillators (NCOs) in the feedback loop.

However, the use of single frequency L1 band signals implies the necessity of taking into account the ionospheric error effect. In fact, even after the application of the Klobuchar and NeQuick ionosphere error correction models to the GPS and Galileo pseudorange measurements, respectively, a resulting ionospheric residual error still remains in the received observations. Therefore, one of the main originality of this work relies on the implementation of a dual-constellation VDFLL architecture, capable of estimating the ionosphere residual error present in the received observations.

A detailed performance comparison between the scalar tracking and VDFLL architecture in terms of positioning performance and code/carrier tracking robustness is performed for a simulated car trajectory in the presence of ionospheric residual errors for an urban environment, which is generated using the wideband DLR model [7]. Specifically, this model generates an artificial scenario representing the characteristics of a given urban environment, where the LOS and multipath echoes are generated per each tracked satellite-user propagation channel.

This paper is organized as follows:

- Section 2 describes in detail the state and observation model of the proposed dual-constellation single-frequency L1/E1 GPS/Galileo VDFLL algorithm.
- Section 3 provides the flowchart of the VDFLL navigation filter, starting from the measurement prediction and the computation of the observation matrix. The main focus of this section is dedicated to the description of the VDFLL measurement innovation vector and code/carrier NCO update formulation.
- Section 4, deals with the test set up description that is split in three main parts: Firstly, the code/carrier tracking parameters for the scalar and vector tracking operation modes are provided. In the second part, a short overview of the DLR urban channel propagation model is given with an emphasis on its output vector including the LOS and multipath echoes parameters. Lastly, the mathematical formulation of the multipath-affected correlator outputs that are further employed for the generation of the discriminator outputs is given.
- The test results for an urban environment representative under the presence of ionosphere residual errors, in terms of position/velocity accuracies and EKF estimation errors, are given in Section 5.
- The main conclusions of this paper and future work will be drawn in Section 6.

2 PROPOSED ARCHITECTURE

In this work, we present the dual constellation single frequency band L1/E1 VDFLL architecture, wherein the code (DLL) and frequency (FLL) tracking loops are coupled through the navigation solution computed by the central extended Kalman filter (EKF).
The reason behind this choice is threefold:

- Firstly, the dual-constellation single frequency vector tracking architecture ensures an increased number of observations that can significantly improve the accuracy and availability of the navigation solution;
- Secondly, an enhanced vehicle dynamics tracking capability of the receiver based on the EKF-estimated receiver dynamics;
- Thirdly, the dual-constellation single frequency vector tracking architecture preserves the low-cost feasibility criteria of a mobile user's receiver.

The proposed VDFLL architecture comprises three sub-modules: the code/carrier tracking loops including the DLL/FLL discriminators, the EKF navigation filter and the code/carrier NCOs update in the feedback loop. The detailed architecture of the proposed L1/E1 VDFLL configuration is sketched in Figure 1, where the code delay- and carrier frequency- related blocks are illustrated in blue and brown, respectively.

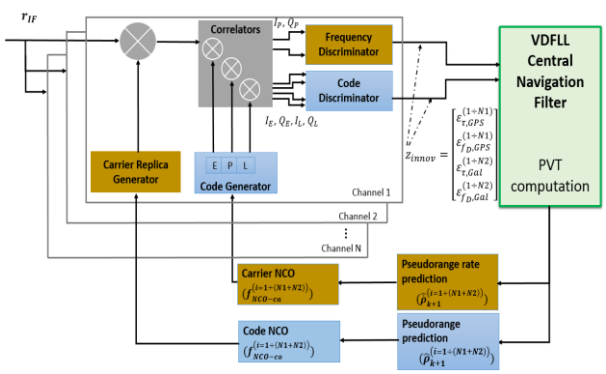

Figure 1 – The proposed L1/E1 VDFLL architecture

As can be observed in Figure 1, the central EKF navigation filter accepts the code $(\boldsymbol{\varepsilon_\tau^{(i)}})$ and carrier $(\boldsymbol{\varepsilon_{f_D}^{(i)}})$ discriminator outputs for each GPS $(\boldsymbol{i = 1 \div N1})$ and Galileo $(\boldsymbol{i = N1 + 1 \div N2})$ tracked channels as its input vector. Contrary to the scalar tracking counterpart, where the code and carrier NCO corrections are generated locally per each channel, in the vectorized architecture the code and carrier NCO update is achieved by projecting the EKF-predicted navigation solution in the pseudorange and pseudorange rate error domains.

2.1 EKF State Model

The use of dual constellation but single frequency L1 band signals does not cancel out the ionosphere effect on the observations. In fact, ionosphere residual errors are still present in each pseudorange measurement even after application of the Klobuchar or NeQuick corrections. Thus, the proposed VDFLL architecture is designed with the objective of estimating the ionosphere residual error affecting each satellite observation.

The chosen state vector model in our EKF navigation filter implementation is the Position, Velocity and Time (PVT) representation, augmented with the ionosphere residual states per each tracking channel (i) for the kth epoch as follows:

$$X_{VDFLL,k} = X_k = \begin{bmatrix} X_{PVT} \\ b_{I-GPS,k}^{(1)} \\ b_{I-GPS,k}^{(2)} \\ \vdots \\ b_{I-GPS,k}^{(N1)} \\ b_{I,k}^{(1)} \\ b_{I-Gal,k}^{(2)} \\ \vdots \\ b_{I-Gal,k}^{(N2)} \end{bmatrix}_{\{8+(N1+N2)\}\times 1} , \qquad (1)$$

where:

- $X_{PVT} = [x, \dot{x}, y, \dot{y}, z, \dot{z}, b_{Rx}, \dot{b}_{Rx}]_{8\times 1}^T$ is the 8x1 absolute PVT state vector, containing the following terms:
  - $[x(k), y(k), z(k)]^T$ and $[\dot{x}(k), \dot{y}(k), \dot{z}(k)]^T$ denote the receiver's position and velocity vectors in the Earth Centered Earth Fixed (ECEF) frame, expressed in $[m]$ and $[m/s]$, respectively;
  - The receiver's clock dynamics comprising the receiver clock bias and drift w.r.t the GPS time $[b_{Rx}, \dot{b}_{Rx}]^T$, expressed in unit of $[m]$ and $[m/s]$, respectively.
- $b_{I-GPS/Gal,k}^{(i)}$ denotes the ionosphere residual error in $[m]$, affecting the pseudorange measurements for the N1 GPS and N2 Galileo tracking channels.

In the PVT state vector only one clock bias state appears since the inter-constellation GPS-Galileo clock offset is considered as provided in a very reliable way by the Galileo navigation message.
For simplicity purpose and according to the EKF state vector of Eq. (1), a separate description of the EKF state model concerning the PVT and ionosphere residual terms will be provided.

2.1.1 EKF PVT State model

The PVT state-space model of the EKF-based navigation filter in the continuous time domain is established as follows:

$$\frac{d}{dt} X_{PVT}(t) = F(t) \cdot X(t) + B(t) \cdot w(t) \qquad (2)$$

where $\frac{d}{dt} X_{PVT}$ denotes the time derivation operation applied to PVT state vector $X_{PVT}(t)$, $F(t)$ is the state transition matrix describing the user's platform and

receiver's clock dynamics, $B(t)$ is the colored noise transition matrix and $w(t)$ is the process noise vector representing the uncertainties affecting the system model. Solving the differential equation above provides the state vector estimation at time t as a function of the state vector at time $t-\tau$ as [10]:

$$\hat{X}(t) = \exp\left(\int_{t-\tau}^{t} F(t)dt\right) \cdot \hat{X}(t-\tau) \quad (3)$$

The discrete state transition matrix Φ_k is then computed as:

$$\Phi_k \approx \exp(F_k \cdot \Delta T) \quad (4)$$

Where $\Delta T = t_{k-1} - t_k$ is the time step between two successive epochs.

The matrix exponential is calculated as the Taylor's power-series expansion of the continuous-time transition matrix F and by truncating it in the first-order solution, the discrete state transition matrix Φ_k is expressed as:

$$\Phi_k = \sum_{n=0}^{+\infty} \frac{F_k^n \cdot \Delta T^n}{n!} \approx I + F_k \cdot \Delta T \quad (5)$$

Finally, the PVT discrete state transition matrix, representing the dynamics of the user's platform and clock, is given by:

$$\Phi_{PVT} = \begin{bmatrix} C_{2\times2} & 0_{2\times2} & 0_{2\times2} & 0_{2\times2} \\ 0_{2\times2} & C_{2\times2} & 0_{2\times2} & 0_{2\times2} \\ 0_{2\times2} & 0_{2\times2} & C_{2\times2} & 0_{2\times2} \\ 0_{2\times2} & 0_{2\times2} & 0_{2\times2} & C_{2\times2} \end{bmatrix}_{8\times8} \quad (6)$$

where:

$$C_{2\times2} = \begin{bmatrix} 1 & \Delta T \\ 0 & 1 \end{bmatrix}. \quad (7)$$

Concerning the process noise vector $\boldsymbol{w}$, the five tuning factors of its continuous-time covariance matrix $\boldsymbol{Q}$ are grouped into two main categories**:**

- *User's dynamics sensitive*: reflecting the user's dynamics uncertainties and including the velocity error variance terms along the three ECEF axes $(\sigma_{\dot{x}}^2, \sigma_{\dot{y}}^2, \sigma_{\dot{y}}^2)$ that are projected in the position domain through the state transition sub-matrix $C_{2\times2}$;
- *Receiver's oscillator noise Power Spectrum Density (PSD)*: including the oscillator's phase noise PSDs affecting the receiver clock bias denoted as σ_b^2 and the oscillator's frequency noise variance σ_d^2. Both these PSD values depend on the Allan variance parameters (h_0, h_{-1} and h_{-2}).

The PVT process noise covariance matrix $Q_{PVT,k} = diag\ [Q_{x,k}, Q_{y,k}, Q_{z,k}, Q_{c,k}]$ in the discrete domain per each entry can be expressed as:

$$Q_{x,k} = \int_{t_{k-1}}^{t_{k-1}+\Delta T} \Phi_x(\mathrm{T}) \cdot \mathrm{Q}_x \cdot \Phi_x{}^{\mathrm{T}}(\mathrm{T})\ dt \quad (8)$$

where Q_x represents the process noise covariance matrix in the continuous time domain for the user's position and velocity along the x axes. Thus, the user's dynamics process noise discretization for the position- and velocity-states along the x-axes is computed as:

$$Q_{x,k} = \int_{t_{k-1}}^{t_{k-1}+\Delta T} \begin{bmatrix} 1 & \Delta T \\ 0 & 1 \end{bmatrix} \cdot \begin{bmatrix} 0 & 0 \\ 0 & \sigma_{\dot{x}}^2 \end{bmatrix} \cdot \begin{bmatrix} 1 & 0 \\ \Delta T & 1 \end{bmatrix} dt \quad (9)$$

Finally:

$$Q_{x,k} = \sigma_{\dot{x}}^2 \cdot \begin{bmatrix} \Delta T^3/3 & \Delta T^2/2 \\ \Delta T^2/2 & \Delta T \end{bmatrix} \quad (10)$$

The same logic is applied to obtain the discrete-time process noise covariance matrix for the y- and z-axes user's position projections:

$$Q_{y,k} = \sigma_{\dot{y}}^2 \cdot \begin{bmatrix} \Delta T^3/3 & \Delta T^2/2 \\ \Delta T^2/2 & \Delta T \end{bmatrix}, \quad (11)$$

and,

$$Q_{z,k} = \sigma_{\dot{z}}^2 \cdot \begin{bmatrix} \Delta T^3/3 & \Delta T^2/2 \\ \Delta T^2/2 & \Delta T \end{bmatrix} \quad (12)$$

The discrete receiver's clock process noise covariance matrix is modelled based on the oscillator's Allan variance parameters and is computed as follows:

$$\begin{aligned} \boldsymbol{Q}_{clk,k} &= \int_{t_{k-1}}^{t_k} \boldsymbol{C}_{2\times2}(t_k,\tau) \cdot \boldsymbol{Q}_{\boldsymbol{clk},\boldsymbol{2}\times\boldsymbol{2}}(\tau) \cdot \boldsymbol{C}_{2\times2}^T(t_k,\tau) d\tau \\ &= \int_{t_{k-1}}^{t_k} \begin{bmatrix} 1 & \Delta T \\ 0 & 1 \end{bmatrix} \cdot \begin{bmatrix} \sigma_b^2 & 0 \\ 0 & \sigma_d^2 \end{bmatrix} \cdot \begin{bmatrix} 1 & 0 \\ \Delta T & 1 \end{bmatrix} \cdot d(\Delta T) \\ &= \begin{bmatrix} \sigma_b^2 \cdot \Delta T + \sigma_d^2 \cdot \Delta T^3/3 & \sigma_d^2 \cdot \Delta T^2/2 \\ \sigma_d^2 \cdot \Delta T^2/2 & \sigma_d^2 \cdot \Delta T \end{bmatrix} \end{aligned} \quad (13)$$

where the receiver's oscillator frequency PSD influence on the clock bias and drift terms are detailed in the following section.

2.1.2 EKF Ionosphere Residual State model

The use of dual constellation but single frequency L1 band signals does not allow the entire correction of the ionosphere delay. Even after the application of the Klobuchar and Nequick ionosphere error correction models to the GPS and Galileo pseudorange measurements, respectively, a resultant ionosphere residual error still remains in the received observations.

The ionosphere residual error is correlated in time and can be modelled as a first order Gauss-Markov (GM) process, having an exponentially decaying autocorrelation function, as proposed by the civil aviation community in [11]. The first-order Gauss-Markov stationary process is expressed in continuous time as follows:

$$\dot{b_I} = -\frac{1}{\tau} \cdot b_I + w_I, \quad (14)$$

where b_I denotes the ionosphere residual GM random process, τ is the ionosphere error correlation time that is set to $1800\ s$ according to the GPS L1 and Galileo E1 MOPS, respectively provided in [11] and [12] and w_I is the process driven noise with zero mean and variance $\sigma_{w_I}^2$.

The discrete time model of the ionosphere residual GM random process $b_{I,k}$ at the kth epoch is expressed as follows:

$$b_{I,k} = e^{-\frac{\Delta T}{\tau}} \cdot b_{I,k-1} + w_{I,k} \tag{15}$$

In discrete time, the process driven noise variance $\sigma_{w_{I,k}}^2$ is deduced from the global GM process using the following relation:

$$\sigma_{w_{I,k}}^2 = \sigma_{iono,k}^2 \cdot \left(1 - e^{-\frac{2\cdot\Delta T}{\tau}}\right) \tag{16}$$

where the standard deviation of the ionospheric residual error $\sigma_{iono,k}$ for the single-frequency GPS L1 and Galileo E1 signals is obtained from the Klobuchar and NeQuick ionosphere correction models, as detailed in the Simulation test section.

Since this work is focused on the proposal and implementation of the VDFLL algorithm, the ionosphere residual error impact on the pseudorange rate measurement and its mathematical formulation is of great interest. The effect of the ionosphere residual error in the pseudorange rate measurement $\left(\dot{b}_{I,k}\right)$ can be deduced through differencing the ionosphere residual error between two consecutive epochs:

$$\dot{b}_{I,k} = \frac{b_{I,k} - b_{I,k-1}}{t_k - t_{k-1}} = \frac{b_{I,k} - b_{I,k-1}}{\Delta T} \tag{17}$$

While, the ionosphere residual rate process driven variance $\sigma_{w,\dot{I}_k}^2$, affecting the carrier tracking loops, is computed as follows:

$$\sigma_{w,\dot{I}_k}^2 \cong \frac{2 \cdot \sigma_{w_k}^2}{\Delta T} = 2 \cdot \sigma_{iono,k}^2 \cdot \left(1 - e^{-\frac{2\cdot\Delta T}{\tau}}\right) \tag{18}$$

2.1.3 Complete VDFLL EKF State model

Combining the discrete state transition matrix relations, related to the PVT and ionosphere residual error terms, respectively provided in Eq. (5), (6) and (14), the complete VDFLL state transition matrix is formulated as:

$$\Phi_{VDFLL,k} = \Phi_k = \begin{bmatrix} \Phi_{8\times8} & 0 & \cdots & 0 \\ 0 & e^{-\frac{\Delta T}{\tau}^{(1)}} & 0 & 0 \\ \vdots & 0 & \ddots & 0 \\ 0 & 0 & 0 & e^{-\frac{\Delta T}{\tau}^{(N)}} \end{bmatrix}_{(8+N)\times(8+N)} \tag{19}$$

where $\Phi_{9\times9}$ is the discrete PVT state transition matrix detailed in Eq. (6) and $e^{-\frac{\Delta T}{\tau}}$ is the exponential decaying coefficient of the ionosphere residual error for each satellite (GPS and Galileo) channel from $i = 1 \div N$, for $N = N_1 + N_2$.

As a consequence, the process noise covariance matrix Q_k should take into consideration the ionospheric disturbance present on the received signal and is expressed as:

$$Q_{VDFLL,k} = Q_k = \begin{bmatrix} Q_{8\times8} & 0 & \cdots & 0 \\ 0 & \sigma_{w,I}^{2\ (1)} & 0 & 0 \\ \vdots & 0 & \ddots & 0 \\ 0 & 0 & \dots & \sigma_{w,I}^{2\ (N)} \end{bmatrix}_{(8+N)\times(8+N)} \tag{20}$$

for which $Q_{8\times8}$ is the discrete process noise covariance matrix comprising the user's dynamics and receiver's oscillator errors presented in Eq. (9) to (13) and $\sigma_{w,I}^{2\ (i)}$ is the ionospheric residual error driven process noise for each satellite channel from $i = 1 \div N$.

2.2 EKF Observation Model

The non-linear relation between the state and the measurement vector is expressed as follows:

$$z_k = h(X_k) + v_k \tag{21}$$

where h is the *non-linear* function relating the measurement z_k to the state X_k and v_k is *the measurement noise vector* that is modelled as a zero-mean uncorrelated Gaussian noise process and independent to the process noise w_k. The measurement vector z_k comprises pseudoranges $\rho^{(i)}$ and Doppler measurements $\dot{\rho}^{(i)}$, output from the code/carrier tracking process for the $i = 1 \div N$ GPS L1/ Galileo E1 tracking channels:

$$z_k = \left[(\rho^{(1)}\ \rho^{(2)}\ \cdots \rho^{(N)}) \vdots (\dot{\rho}^{(1)}\ \dot{\rho}^{(2)}\ \cdots \dot{\rho}^{(N)})(k)\right]_{2N\times1} \tag{22}$$

Including the ionosphere residual error impact, the GNSS pseudorange measurements of a given satellite i (from the GPS ($N1$) and Galileo ($N2$) satellites in-view) at epoch k are rewritten as:

$$\rho^{(i)}(k) = \begin{cases} R_{GPS}^{(i)} + b_{Rx} + b_{I-GPS}^{(i)} + n_{\rho,GPS}^{(i)}(k) & 0 < i \le N1 \\ R_{Gal}^{(i)} + b_{Rx} + b_{I-Gal}^{(i)} + n_{\rho,Gal}^{(i)}(k) & N1 < i \le N2 \end{cases} \tag{23}$$

where:

$$R_{GPS/Gal}^{(i)}(k) = \sqrt[2]{\left(x_s^{(i)} - x\right)^2 + \left(y_s^{(i)} - y\right)^2 + \left(z_s^{(i)} - z\right)^2}\,(k)$$

is the GPS and Galileo satellite-to-user geometric distance at the current epoch k.

While the remaining M-entries of the measurement vector, constituted by the Doppler measurements, are modelled as:

$$\begin{aligned} \dot{\rho}_{GPS/Gal}^{(i)}(k) = &\left(\dot{x}_s^{(i)}(k) - \dot{x}(k)\right) \cdot a_x^{(i)}(k) \\ &+ \left(\dot{y}_s^{(i)}(k) - \dot{y}(k)\right) \cdot a_y^{(i)}(k) \\ &+ \left(\dot{y}_s^{(i)}(k) - \dot{y}(k)\right) \cdot a_y^{(i)}(k) \\ &+ c \cdot \dot{b}_{Rx}(k) + b_{I-GPS/Gal}^{(i)}(k) + n_{\dot{\rho}}^{(i)}(k) \end{aligned} \tag{24}$$

where

- the $\left(a_x^{(i)}, a_y^{(i)}, a_z^{(i)}\right)$ are the LOS projections along the three ECEF axes ($l = x, y, z$), given by:

$$a_l^{(i)} = \frac{\left(X_s^{(i)}(k) - X(k)\right)}{R^{(i)}(k)} \tag{25}$$

- $X = (x, y, z)$ and $X_s^{(i)} = (x_s^{(i)}, y_s^{(i)}, z_s^{(i)})$ being the 3D i^{th} satellite and user's position vectors expressed in the ECEF frame, respectively;
- $\dot{X} = (\dot{x}, \dot{y}, \dot{z})$ and $X_s^{(i)} = (\dot{x}_s^{(i)}, \dot{y}_s^{(i)}, \dot{z}_s^{(i)})$ denote the 3D i^{th} satellite and user's velocity vectors expressed in the ECEF frame, respectively;
- b_{Rx} denote the user's clock bias w.r.t the GPS time expressed in $[m]$;
- $\dot{b}_{Rx}$ represents the user's clock drift in $\left[\frac{m}{s}\right]$;
- $b_{I-GPS/Gal}^{(i)}$ and $b_{\dot{I}-GPS/Gal}^{(i)}$ denote the ionosphere residual and residual rate errors in unit of $[m]$ and $[m/s]$ affecting the GPS and Galileo code and carrier measurements, respectively;
- $(n_{\rho_{j,k}}, n_{\dot{\rho}_{j,k}})$ denote the zero-mean Gaussian-distributed noises affecting the pseudorange and Doppler measurements, respectively.

The measurement noise vector v_k is modelled as a zero-mean uncorrelated Gaussian noise process and independent to the process noise w_k:

$$\begin{aligned} E[v_k] &= 0 \\ E[v_k \cdot w_l^T] &= 0 \\ E[v_k \cdot v_l^T] &= R_k \cdot \delta_{kl}, \qquad \text{for all } k \text{ and } l \end{aligned} \tag{26}$$

where δ_{kl} denotes the Kronecker's delta and R_k represents the *measurement noise covariance matrix*.

In our vector tracking algorithm, the measurements are interpreted as the addition of the discriminator outputs and the measurement prediction. Assuming that the code delay and carrier frequency errors are small enough to fall into the discriminator linear region, the discriminator output can then be directly interpreted as the EKF innovations.

Recalling from the statistical theory that the derivative of a 1st order Gauss-Markov process is a Gaussian noise [9], the EKF filter is not capable of observing and later estimating the ionosphere residual rate error effect on the Doppler measurements. In order to cope with this issue, the measurement covariance matrix terms related to the Doppler measurements are increased by the ionosphere residual rate process driven variance $\sigma_{w,\dot{I}_k}^2$ from Eq. (18). The measurement noise covariance matrix has in the main diagonal the following entries:

$$\boldsymbol{R}_k = \begin{cases} \sigma^{2\,(i)}_{code}(k) & for\ 1 \le i \le N \\ \sigma^{2\,(i)}_{carrier}(k) + \sigma_{w,\dot{I}_k}^{2\ (i)} & for\ 1 \le i \le N \end{cases} \tag{27}$$

where the first entries refer to the pseudorange (code) measurement error variance terms for the tracked GPS and Galileo satellites, while the second terms are related to the pseudorange rate (carrier) error variances for all tracked satellites i.

3 VDFLL EKF FLOWCHART

The detailed flowchart of the VDFLL EKF estimation process is illustrated in Figure 2, where it can be noticed that the EKF estimation equations fall in two categories:

- *State prediction (time update)* equations, performing the propagation in time of the state vector X and its covariance matrix P from the previous time epoch $k-1$ to the current one k;
- *Measurement update (correction)* equations, refining the predictions by feeding the measurement innovation vector into the filter and thus, obtaining the improved *a posteriori* estimates $(X_{k|k}, P_{k|k})$.

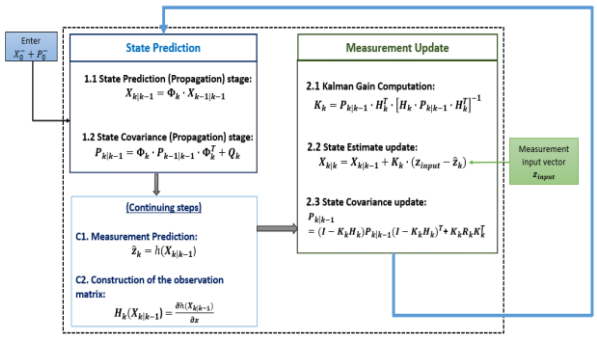

Figure 2 – The complete flowchart of the EKF recursive operation constituted by the state prediction (in blue) and measurement update (in green) blocks.

The EKF measurement update process requires the computation of two intermediary steps, such as the measurement prediction and observation matrix H_k calculation.

3.1 The Measurement Matrix H_k generation

The predicted measurement vector $\hat{\boldsymbol{z}}_k$ is computed by applying the non-linear observation function h on the state vector prediction $\boldsymbol{X}_{k|k-1}$ and includes the predicted pseudorange $\hat{\rho}_k^{(i)}$ and pseudorange rates $\hat{\dot{\rho}}_k^{(i)}$ for each satellite in-view $i = 1 \div N$:

$$\begin{aligned} z_k = \big[& (\hat{\rho}^{(1)}\ \hat{\rho}^{(2)}\ \cdots \hat{\rho}^{(N)}) \\ & \vdots\ (\hat{\dot{\rho}}^{(1)}\ \hat{\dot{\rho}}^{(2)}\ \cdots \hat{\dot{\rho}}^{(N)})(k) \big]_{2N\times 1} \end{aligned} \tag{28}$$

The only difference w.r.t the scalar tracking EKF-based solution consists on the addition of the predicted ionosphere residuals errors $\hat{b}_{I,k}^{(i)}$ to the predicted ranges and user's clock bias terms as:

$$\begin{aligned} &\hat{\rho}^{(i)}(k) \\ &= \begin{cases} \hat{R}_k^{(i)} + \boldsymbol{X}_{k|k-1}(7) + \boldsymbol{X}_{k|k-1}(8+i) & 0 < i \le N1 \\ \hat{R}_k^{(i)} + \boldsymbol{X}_{k|k-1}(7) + \boldsymbol{X}_{k|k-1}(8+i) & N1 < i \le N \end{cases} \end{aligned} \tag{29}$$

where $\hat{R}_k^{(i)}$ is the predicted i^{th} satellite-user distance, $\boldsymbol{X}_{k|k-1}(7)$ denotes the predicted clock biases w.r.t the GPS time scale and $\boldsymbol{X}_{k|k-1}(8+i) = \hat{b}_{I,k}^{(i)}$ refers to the predicted ionosphere residual error positioned in the $8+i$ element of the state vector prediction $\boldsymbol{X}_{k|k-1}$, after the 8 PVT states. Whereas, the predicted pseudorange rate $\hat{\dot{\rho}}_k^{(i)}$ is provided as:

$$\hat{\rho}_k^{(i)} = \left(\dot{x}_s^{(i)}(k) - \boldsymbol{X}_{k|k-1}(2)\right) \cdot \hat{a}_x^{(i)}(k) + \left(\dot{y}_s^{(i)}(k) - \boldsymbol{X}_{k|k-1}(4)\right) \cdot \hat{a}_y^{(i)}(k) + \left(\dot{z}_s^{(i)}(k) - \boldsymbol{X}_{k|k-1}(6)\right) \cdot \hat{a}_z^{(i)}(k) + \boldsymbol{X}_{k|k-1}(8) + \frac{\left(\boldsymbol{X}_{k|k-1}(8+i) - \boldsymbol{X}_{k-1|k-2}(8+i)\right)}{\Delta T} \quad (30)$$

Where:

- $\left(\boldsymbol{X}_{k|k-1}(2), \boldsymbol{X}_{k|k-1}(4), \boldsymbol{X}_{k|k-1}(6)\right)$ is the predicted user velocity vector in ECEF frame;
- $\hat{a}_{x,y,z}^{(i)}$ denote the predicted LOS projections along the three ECEF axes;
- $\boldsymbol{X}_{k|k-1}(8)$ refers to the predicted clock drift in $\left(\frac{m}{s}\right)$;
- $\frac{\left(\boldsymbol{X}_{k|k-1}(8+i) - \boldsymbol{X}_{k-1|k-2}(8+i)\right)}{\Delta T}$ denotes the contribution of the predicted ionosphere residual rate computed as the change rate between the ionosphere residual estimations of two consecutive epochs *k-1* and *k*.

Finally, the VDFLL observation matrix accounting for the ionosphere residual errors is formulated as:

$$H_{VDFLL,k} = H_k = \begin{bmatrix} H_{\rho^{(1)},1\times 8} & 1^{(1)} & \cdots & 0 \\ H_{\rho^{(i)},1\times 8} & 0 & \ddots & 0 \\ H_{\rho^{(N)},1\times 8} & 0 & \dots & 1^{(N)} \\ H_{\dot{\rho}^{(1)},1\times 8} & 0 & \cdots & 0 \\ H_{\dot{\rho}^{(i)},1\times 8} & 0 & \ddots & 0 \\ H_{\dot{\rho}^{(N)},1\times 8} & 0 & 0 & 0 \end{bmatrix}_{(2N)\times(8+N)} \quad (31)$$

where $H_{\rho^{(1)},1\times 8}$ and $H_{\dot{\rho}^{(1)},1\times 8}$ are row vectors that comprise the pseudorange and pseudorange rate predictions partial derivatives w.r.t the 8 PVT states, provided in [13].

3.2 VDFLL EKF Innovation vector

The proposed dual constellation VDFLL algorithm operates at a 50 Hz update rate matching with the scalar code/carrier tracking update frequency. The code delay and frequency carrier estimation process are achieved per channel basis as in the scalar configuration, however in the designed vectorized architecture, the code and frequency discriminator outputs will be directly fed to the EKF navigation filter as its measurement innovation vector $z_{innov,k}$, as shown in Eq. (32).

As explained earlier, this is valid under the assumption that the code delay and carrier frequency errors fall into their discriminator's linear region and when the EKF-computed code and carrier NCO feedback loops to each satellite channel are performed at the code and carrier accumulation rate.

The measurement innovation vector $\boldsymbol{z}_{innov,k}$ at epoch k includes the pseudorange and pseudorange rate errors $\varepsilon_{code/carr}$ for each tracking channel $i = 1 \div N$ that are computed from the code and carrier discriminator functions using the following expression:

$$\begin{aligned} z_{innov,k} &= z_k - \hat{z}_k \\ &= \left(h(X_{k|k-1}) + \varepsilon_{code/carr}\right) - h(X_{k|k-1}) \\ &= [\left(\frac{c}{f_{code}}\right) \cdot \left(\varepsilon_{\tau,GPS}^{(i=1\div N1)} \; \varepsilon_{\tau,Gal}^{(i=(N1+1)\div N)}\right) \vdots \\ &\left(\frac{c}{f_{carr}}\right) \cdot \left(\varepsilon_{f_D,GPS}^{(i=1\div N1)} \; \varepsilon_{f_D,Gal}^{(i=(N1+1)\div N)}\right)(k)]_{2N\times 1} \end{aligned} \quad (32)$$

where the first N terms for the GPS N_1 and Galileo $[(N_1+1) \div N]$ channels, related to the pseudorange errors, are expressed in $[m]$ and computed from the code discriminator outputs ε_τ , while the remaining N entries of the measurement innovation vector denote the pseudorange rate errors in $[m/s]$ obtained from the frequency discriminators.

3.3 VDFLL NCO Update

The Doppler frequency correction $f_{NCO-ca}^{(i)}$ per each tracking channel *i*, closing the feedback loop to the carrier NCO, is computed by projecting the predicted velocity- and clock drift errors states in the pseudorange rate error domain as:

$$f_{NCO-ca}^{(i)} = \frac{f_{carr}}{c} \cdot \hat{\rho}^{(i)}(k) \; (Hz) \quad (33)$$

where: $f_{carr} = 1{,}57542\ GHz$ refers to GPS L1 & Galileo E1 carrier frequency and $c \cong 3 \cdot 10^8$ is the speed of light in (m/s).

On the other hand, the relative code NCO command for each channel i is forwarded to successive tracking epoch by taking the difference between the pseudorange predictions of two consecutive measurement epochs, denoted as $\hat{\rho}^{(i)}(k+1)$ and $\hat{\rho}^{(i)}(k)$, respectively:

$$\Delta f_{NCO-co}^{(i)}(k+1) = f_{code} \cdot \frac{\left(\hat{\rho}^{(i)}(k+1) - \hat{\rho}^{(i)}(k)\right)}{c \cdot \Delta T} \left(\frac{chip}{s}\right) \quad (34)$$

Therefore, the code NCO frequency can be expressed by the addition of the relative code NCO to the nominal chipping frequency f_{code}, expressed as:

$$f_{NCO-co}^{(i)}(k+1) = f_{code} + \Delta f_{NCO-co}^{(i)}(k+1) \quad (35)$$

4 TEST SETUP

Within the scope of this research, a realistic dual-constellation dual-frequency GNSS signal emulator comprising the navigation module has been developed in C language platform to improve the processing speed. The term emulator comes from the fact that the received GNSS signals are simulated at the correlator output level. The developed signal emulator is a powerful tool for flexible and reliable GNSS receiver testing, for which all the processing blocks from the GNSS signals' correlation function, passing through the channels' tracking module and up to the different navigation algorithms are all designed in a modular manner. This allows easy modifications according to the test scenarios and user motion and with the objective of providing an efficient switch between the scalar- and vector tracking operation modes.

Two distinct GNSS receiver architectures will be analyzed with the scope of performance comparison:

- The proposed L1/E1 VDFLL EKF architecture working at $\Delta T = 20\ ms$ integration time and thus providing 50 Hz code and carrier frequency updates.
- Scalar tracking employing a 3rd order loop PLL and a DLL, with a KF positioning module for the PVT computation operating at the same rate as for the VDFLL EKF case (50 Hz).

4.1 Simulation Parameters

The simulations performed in this work are related to a car trajectory in Toulouse urban area that was generated based on the data collected during a real test campaign in Toulouse using a reference trajectory computed by the NovAtel's SPAN receiver mounted on the car. It must be noted that only the simulated car path of 600 seconds duration is taken from this trajectory that is illustrated in Figure 3. The simulated reception conditions are that of a complete urban multipath model integrated to the receiver model in the presence of ionosphere residual errors. In both test scenarios, there is maximum of 13 simultaneously tracked GPS L1 and Galileo E1 channels during the 10 minutes urban trajectory.

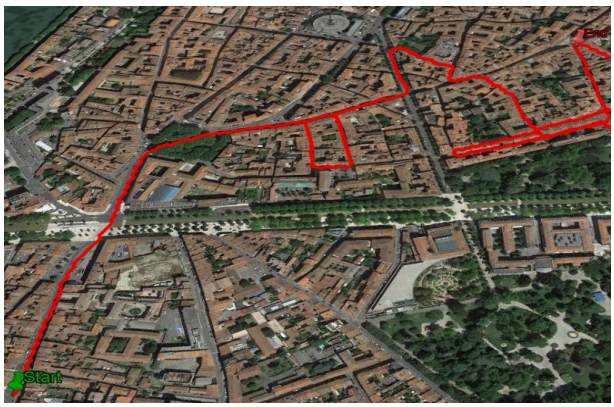

Figure 3 – The reference car trajectory in Toulouse city center.

The receiver parameters used during the tests, defining the scalar (ST) and the vector tracking (VT) loop design are summarized in Table 1.

Table 1 – Code and Carrier tracking parameters for the scalar and vector tracking architectures

L1/E1 Code Tracking Parameters	
DLL order (for scalar)	1st
DLL noise bandwidth ($\mathbf{B_{DLL-n}}$) (for scalar)	1 Hz
DLL update period	0.02 s
Code delay discriminator	Early Minus Late Power (EMLP)
GPS L1 chip spacing ($\mathbf{k_{Cs-L1}}$)	0.5 chips
GAL E1 chip spacing ($\mathbf{k_{Cs-E1}}$)	0.2 chips

L1/E1 Carrier Tracking Parameters	
Scalar Configuration	
PLL order (for scalar)	3
PLL noise bandwidth ($\mathbf{B_{PLL-n}}$) (for scalar)	10 Hz
PLL period	0.02 s
Carrier phase discriminator	Atan 2
Vectorized Architecture	
Carrier frequency period	0.01 s
Carrier frequency discriminator	Cross Dot Product

A detailed performance comparison between the scalar and vectorized configurations will be assessed in two different levels:

- ***Navigation level***: expressed in terms of user's position and velocity estimation accuracies, and their errors statistics expressed in along- and cross track coordinates;
- ***Channel level:*** indicated by the code delay and carrier Doppler frequency estimation errors and their standard deviations in degraded signal reception conditions.

The simulations herein presented use the GPS and Galileo constellations in the L1 band, taking into consideration the binary phase shift keying BPSK(1) modulation for GPS L1 and the binary offset carrier modulation BOC(1,1) for the pilot signals. An RF front-end with a 24 MHz bandwidth (double-sided) is assumed. Four main differences can be envisaged between the scalar and vector tracking operation modes.

- Firstly, the KF navigation filter in the scalar receiver operates on locked satellites whereas the VDFLL algorithm takes use of the measurements coming from all the satellites in view (with a specific weighting scheme);
- Secondly, the satellite lock detection test is implemented through the C/N_0 estimator [14] and under outage conditions, a hot re-acquisition process of 1 second duration is applied with initial code errors related to the L1 and E1 code autocorrelation sharpness and initial frequency errors equal to Doppler bin size of 25 Hz. Contrary to the scalar tracking configuration, a "sliding-window" C/N_0 estimation function is implemented in the vector tracking algorithm that removes the need of a re-acquisition module;
- Thirdly, the VDFLL state vector is augmented with the ionosphere residual error per tracking channel, while the classic PVT state vector is employed for the scalar architecture;
- Last but not least, the tracking error variances in the open-loop configuration are fed to the VDFLL measurement covariance matrix, since the code/carrier feedback is closed after the EKF

position update. Whereas for the scalar tracking operation mode, the classic DLL and PLL tracking error variances are included into the scalar measurement covariance matrix R_k for each locked satellite as in [15].

In the proposed VDFLL architecture, an Early Minus Late Power (EMLP) discriminator has been chosen for both the GPS BPSK and Galileo E1 BOC (1,1) channels. The code tracking error variance in the presence of thermal noise and in the open-loop configuration is computed as [13]:

$$\sigma^{2}{}^{(i)}_{co_{VDFLL}}(k) = \left(\frac{c}{f_{code}}\right)^2 \cdot \frac{d \cdot T_c}{2 \cdot \alpha \cdot {}^{C}/_{N_{0_{est}}}{}^{(i)} \cdot T_{DLL}} [m^2] \qquad (36)$$

The FLL tracking error variance of the Cross-Product (CP) discriminator in the open-loop configuration is given by:

$$\sigma^{2}{}^{(i)}_{ca_{VDFLL}}(k) = \left(\frac{c}{f_{carr}}\right)^2 \cdot \left(\frac{1}{{}^{C}/_{N_0}{}^{3(i)}_{est} \cdot T_{FLL}}\right)\left[\frac{m^2}{s^2}\right], \qquad (37)$$

where:

- T_{DLL} and T_{FLL} denote the code and carrier filter integration interval equal to 20 ms;
- C_s is the code chip spacing (0.5 chips for GPS L1 and 0.2 chips for Gal E1 BOC (1,1);
- α is a coefficient reflecting the sharpness of the code autocorrelation function (1 for BPSK(1) and 3 for BOC (1,1));
- $C/N_{0_{est}}$ refers to the estimated carrier-to-noise ratio from the tracking loop of the incoming signal from the ith tracking channel;
- $f_{code} = 1.023\ Mhz$ and $f_{carr} = 1.57542\ GHz$ denote the L1/E1 code chipping rate and carrier frequency, respectively.

It should be reminded that the ionosphere residual error rate variance is added to the carrier tracking error variance in Eq. (37) as presented in Eq. (27).

4.2 Urban Multipath Generation Model

In this work, an urban channel model has been used to generate the amplitude (A_i), delay (τ_i) and phase (φ_i) of each LOS and multipath echoes. This model, known as the DLR Land Mobile Multipath Channel Model (LMMC), was developed thanks to an extensive measurement campaign conducted by DLR in 2002. Moreover, it is a freely accessible algorithm for academic purposes that can be downloaded from the DLR website [7], [8]. This model generates an artificial scenario having the urban environment characteristic including potential obstacles to the received GNSS signal such as trees, buildings, lampposts, as given in Figure 4. In the urban channel configuration, only one satellite at a constant azimuth and elevation angle is simulated at a time. The following parameters are loaded into this model:

- The urban scenario parameters, required to reproduce a typical city street, which include the road width, buildings' height and the trees/lampposts' heights and diameters. All these obstacles are statistically generated.
- The receiver speed and heading angle;
- The satellite elevation and azimuth angles in degrees.

The direct ray (LOS signal) follows a deterministic model determined by the obstacles along the user's trajectory and the LOS amplitude, delay and phase are obtained by ray tracing and geometric techniques. The NLOS echoes are generated in a one by one manner, where each multipath ray is associated with a reflector that is generated following a statistical model.
Furthermore, the number of echoes and their life span are statistical variables depending on the satellite elevation angle. The urban environment conditions are generated for each GPS and Galileo tracked satellite by feeding their elevation and azimuth angles to the modified DLR urban channel.

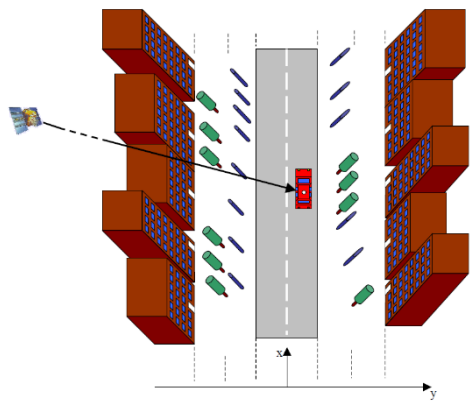

Figure 4 – Artificial urban scenario generated by the DLR urban propagation channel model [7].

In the scenario generation process, the vehicle is set to drive in the middle of the road with the antenna height at 2 m and the building average height set to 10 m, while for coherency issues, the car speed and heading angle is read from the reference trajectory at a sampling frequency equal to the VDFLL position update. During the reference car trajectory, 13 GPS and Galileo satellites are jointly tracked by the receiver. The multipath power delay profiles (PDPs) have been constructed in order to clearly illustrate whether the tracked satellites are in LOS or NLOS reception conditions during the 30000 epochs (600 s · 50 Hz/s), as illustrated in Figure 5 for two different PRNs. The color code is an indicator of the multipath echo's power attenuation w.r.t. the ideal open sky LOS power, where the blue (low signal power) and the red (high signal power) in the near echo region (from $0 - 5\ m$) represent the NLOS and LOS satellite condition, respectively.

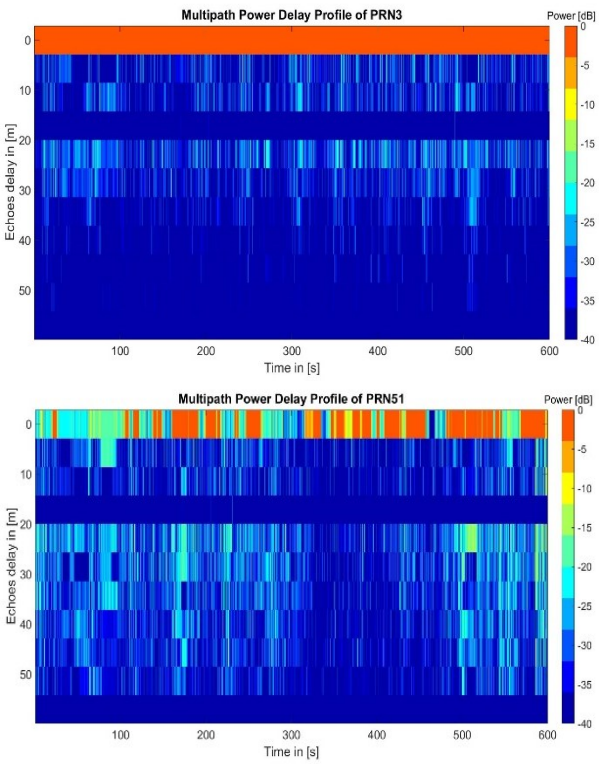

Figure 5 – Multipath power delay profile for a: a) LOS (PRN3); b) NLOS (PRN 51) tracked satellite.

As it can be observed, the PRN3 satellite denotes a LOS satellite due to its high signal power from the LOS ray illustrated in red color. Whereas, PRN14 represents a NLOS satellite based on the green/blue color code with short transitions to the LOS state along the car trajectory. Contrary to the scalar receiver, where the NLOS satellites do not pass the lock detection test, in the VDFLL architecture they are all directly fed to the navigation filter but de-weighted up to a certain level by the EKF measurement covariance matrix R_k.

4.3 Multipath-affected Correlator Outputs

The simulation tool that has been used to test the proposed vectorized architecture is a high-fidelity GNSS receiver simulator that is based on the fine modeling of the correlator outputs. As such, it thus does not require the generation of the actual signals, but only of the corresponding correlator outputs. It is thus extremely important to be able to reproduce very accurately the effect of the error sources of interest on the correlator outputs.
In the tracking stage, the generation of the correlator outputs is certainly affected by the LOS and multipath echoes that increase the code delay and carrier frequency estimation errors. For a clearer understanding of the measurement generation process, a short description of a channel model specifically developed for GNSS applications in urban environments will be given.

The generated database of the received signal rays, obtained from the DLR urban channel model, consists of time series of amplitude, delay and phase of the LOS ray and NLOS echoes received from the satellites in-view elevation and azimuth angles. In order to obtain a realistic vehicle urban scenario coherent with the reference car trajectory fed to the EKF navigation filter, several modification were applied to the DLR model. Firstly, the DLR urban trajectory was generated at a sampling frequency equal to the VDFLL correlation duration rate. Secondly, this model was adapted in such a manner that it can also provide the Doppler frequency of the LOS ray and NLOS echoes, as an output vector for each epoch k:

$$\begin{aligned} mult_k &= [(A_{LOS}, \tau_{LOS}, \varphi_{LOS}, f_{D_{LOS}})_i \vdots \\ &= (A_{NLOS}, \tau_{NLOS}, \varphi_{NLOS}, f_{D_{NLOS}})_j(k)] \end{aligned} \tag{38}$$

Where:

- $(A_{LOS}, \tau_{LOS}, \varphi_{LOS}, f_{D_{LOS}})_i$ denotes the LOS rays' amplitude, delay, phase and Doppler frequency for $(i = 1 \div n_{LOS})$;
- $(A_{NLOS}, \tau_{NLOS}, \varphi_{NLOS}, f_{D_{NLOS}})_j$ denotes the NLOS rays' $(j = 1 \div nr_NLOS)$ amplitude, delay, phase and Doppler frequency for $(j = 1 \div n_{NLOS})$;

It must be noted that the DLR model provides up to three LOS rays, due to the diffraction effects occurring for certain geometries.

Furthermore, the LOS and NLOS echoes information, given above in Eq. (38), is fed in the tracking stage at the correlator output level per each satellite in view, following classical models of the correlator outputs (for the mth satellite):

$$\begin{aligned} IX_m &= \sum_{i=1}^{n_{LOS}} A_{i,LOS} \cdot R\left(\varepsilon_{\tau_{i,LOS}} + d_X\right) \cdot \cos\left(\varepsilon_{\varphi_{i,LOS}}\right) \\ &\quad \cdot \operatorname{sinc}\left(\pi \cdot \varepsilon_{f_{D_{i,LOS}}} \cdot T_s\right) \\ &\quad + \sum_{i=1}^{n_{NLOS}} A_{i,NLOS} \cdot R\left(\varepsilon_{\tau_{i,NLOS}} + d_X\right) \cdot \cos\left(\varepsilon_{\varphi_{i,NLOS}}\right) \\ &\quad \cdot \operatorname{sinc}\left(\pi \cdot \varepsilon_{f_{D_{i,NLOS}}} \cdot T_s\right) + n_{IX,m} \\ QX_m &= \sum_{i=1}^{n_{LOS}} A_{i,LOS} \cdot R\left(\varepsilon_{\tau_{i,LOS}} + d_X\right) \cdot \sin\left(\varepsilon_{\varphi_{i,LOS}}\right) \\ &\quad \cdot \operatorname{sinc}\left(\pi \cdot \varepsilon_{f_{D_{i,LOS}}} \cdot T_s\right) \\ &\quad + \sum_{i=1}^{n_{NLOS}} A_{i,NLOS} \cdot R\left(\varepsilon_{\tau_{i,NLOS}} + d_X\right) \cdot \sin\left(\varepsilon_{\varphi_{i,NLOS}}\right) \\ &\quad \cdot \operatorname{sinc}\left(\pi \cdot \varepsilon_{f_{D_{i,NLOS}}} \cdot T_s\right) + n_{QX,m} \end{aligned} \tag{39}$$

Where:

- X indicates the Early (E), Prompt (P) and Late (L) code replicas shifted by d , depending on the chip spacing T_c as follows:

$$d_X = \begin{Bmatrix} -T_c/2 & if\ X = E \\ 0 & if\ X = P \\ T_c/2 & if\ X = L \end{Bmatrix} \tag{40}$$

- The channel errors including the code delay, carrier phase and frequency errors $(\varepsilon_{\tau_{i,LOS/NLOS}}, \varepsilon_{\varphi_{i,LOS/NLOS}}, \varepsilon_{f_{D_{i,LOS/NLOS}}})$, respectively computed as the difference between the LOS/NLOS related data and the

corresponding VDFLL-estimated values in the feedback loop per each channel, expressed as:

$$\begin{aligned} \varepsilon_{\tau_{i,LOS/NLOS}} &= \tau_{i,LOS/NLOS} - \tau_{est} \\ \varepsilon_{\varphi_{i,LOS/NLOS}} &= (\varphi_0 + \varphi_{i,LOS/NLOS}) - \varphi_{est} \\ \varepsilon_{f_{D\,i,LOS/NLOS}} &= f_{D\,i,LOS/NLOS} - f_{D\,est} \end{aligned} \quad (41)$$

for φ_0 denoting the signal's initial phase;

- $n_{IX,m}$ and $n_{QX,m}$ represent the In Phase and Quadrature correlator output noise terms of the mth tracked channel, respectively, added according to the correlator's noise covariance matrix.

5 TEST RESULTS

In this section, the simulation performance comparison is analyzed in details between the proposed VDFLL algorithm and the scalar tracking architecture with the KF navigation module, focusing on the along and cross track errors and code/carrier tracking channel estimation accuracies. This analysis is provided for the urban environment representative with the inclusion of the multipath channels' parameters from the above described model into the GNSS signal emulator and the presence of the ionosphere residual errors. As previously stated, the ionosphere residual errors affecting the tracking channels are estimated by the VDFLL navigation filter. However, there is no a priori knowledge of the ionosphere residual errors magnitude. For this matter, an adaptive state covariance matrix P is employed for the ionosphere residual states according to the standard deviation of the ionospheric error σ_{iono}, computed based on the mapping function as presented in [11] and [12].

The position and velocity error comparison between the scalar tracking (ST) + KF positioning module at 50 Hz and the VDFLL algorithm are respectively presented in Figure 6 and Figure 7. Both figures present the EKF estimation errors along the entire trajectory: in blue the VDFLL and in red the KF with scalar tracking. Moreover, the blue and red dotted curves denote the 2σ covariance bounds, where σ is the estimation error covariance estimated by the Kalman Filter for the VDFLL and scalar tracking receivers, respectively.

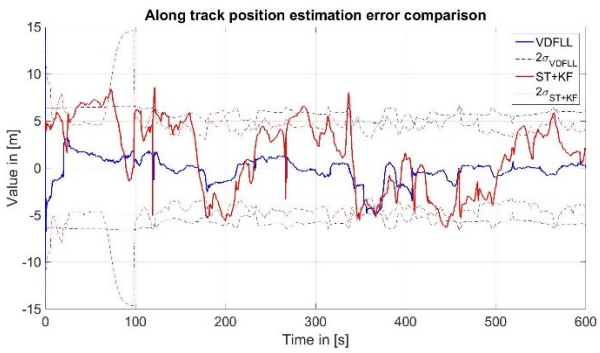

a)

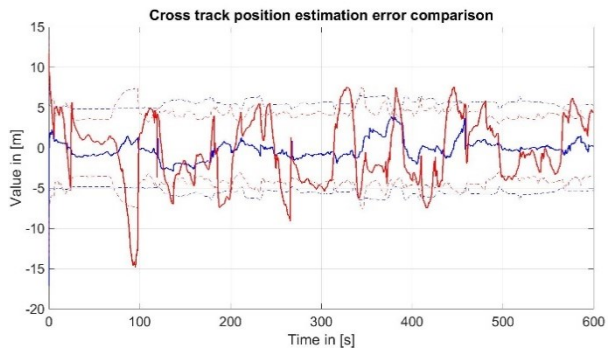

b)

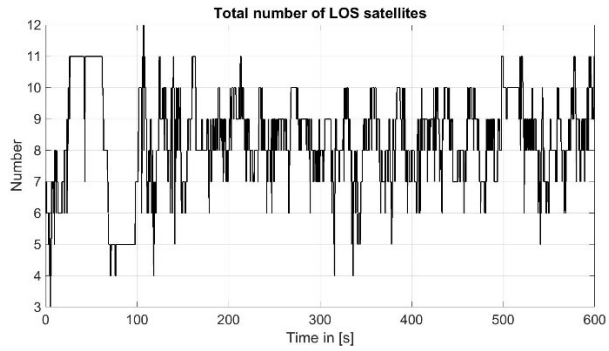

c)

Figure 6 – Position error comparison between the scalar tracking receiver (in red) and the VDFLL algorithm (in blue) for the: a) along track error [m]; b) cross track error [m] and c) Total number of LOS satellites.

The position error plots in the vehicle frame (along and cross track coordinates), illustrated in Figure 6 a) and b), demonstrate a clear stability of the VDFLL-computed navigation solution, expressed in terms of the low position error variations along the trajectory. This reflects the VDFLL capability of estimating the ionosphere residuals and at the same time coping with the multipath conditions. A significant position error of nearly 13 m is observed for the scalar tracking receiver (in red) in the cross track coordinate from the 70th to the 100th epoch, which coincides with strong satellite outage event as illustrated in Figure 6 c). Furthermore, the ST+EKF covariance bounds are significantly increased during this period due to the higher position estimation uncertainty since only four "good" measurements from the four locked LOS satellites are used for the navigation solution computation. On the contrary, the proposed VDFLL algorithm assures a positioning stability and tighter confidence bounds related to the inter-channel aiding achieved by the VDFLL EKF filter. Finally, it can be seen that the vector architecture better assesses the confidence on the computed position.

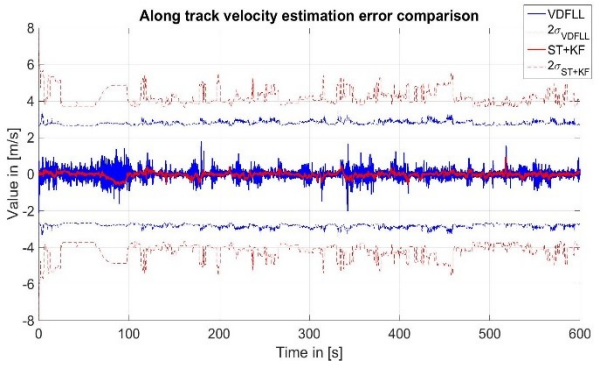

a)

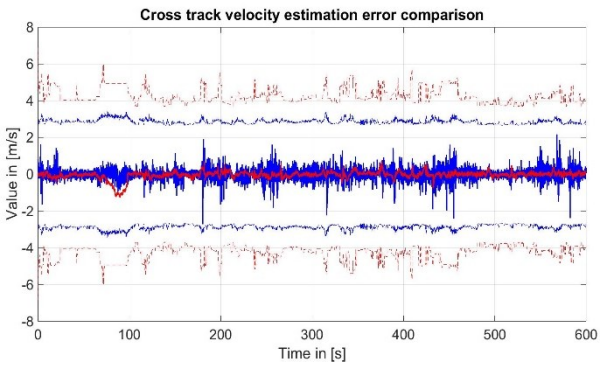

b)

Figure 7 – Velocity error comparison between the scalar tracking + KF positioning module @ 50 Hz (in red), the VDFLL algorithm (in blue) for a car trajectory under multipath and ionosphere presence for the: a) along track error [m]; b) cross track error [m].

A higher VDFLL performance is also noticed in the along and cross track velocity estimates but at a lower order of magnitude compared to the position domain, as illustrated in Figure 7. The VDFLL-estimated along and cross track velocities are noisier compared to the ST+EKF estimations, which is related to the use of frequency discriminators whereas PLLs are employed by the scalar receiver.

For the two receiver's configuration under study, the following statistical parameters are computed:

- The mean of the estimation error, computed as a function of the time.
- The Root Mean Square of the estimation error, referred to as the empirical RMS;

In the framework of this research, the focus is directed toward the filter's accuracy performance assessment. This accuracy limit is supposed to represent the 95% confidence level that contains the estimation error of the considered parameter along the car trajectory. The detailed performance analysis concerning the navigation error statistics are summarized in
Table **2**.

Table 2 – Navigation error statistics for the scalar tracking + KF position module @50 Hz and the proposed VDFLL technique.

	Scalar + KF			VDFLL		
	E[]	RMS[]	95%	E[]	RMS[]	95%
Position errors [m]						
Along track	1.5	4.2	6.9	0.2	1.4	3.1
Cross track	0.5	4.3	7.2	0.1	1.2	2.5
Velocity errors [m/s]						
Along track	~0	0.2	0.5	~0	0.2	0.3
Cross track	~0	0.3	0.6	~0	0.1	0.4

The navigation performance robustness of the proposed VDFLL technique is dedicated to its capability of estimation the ionosphere residual error even for a NLOS satellite channel and correctly following its evolution, based on the EKF-estimated NCO feedback loop, as illustrated in Figure 8.

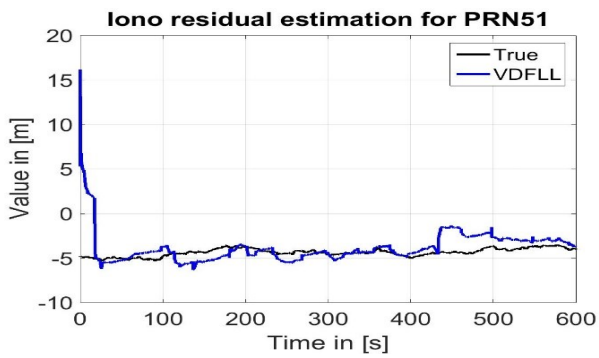

a)

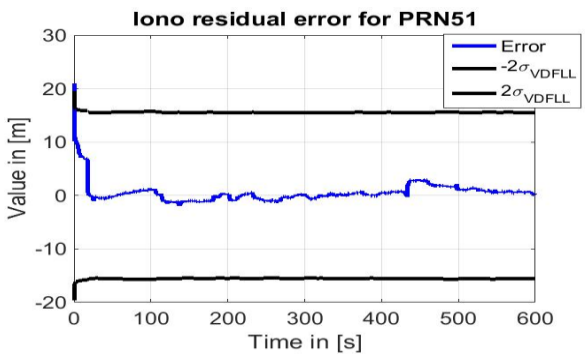

b)

Figure 8 – a) Ionosphere residual error estimation evolution (blue) w.r.t the true residual (black); b) its estimation error and EKF covariance bounds for the Galileo PRN 51 ionosphere residual error.

The performance analysis in the signal level for the LOS satellite, namely Galileo PRN 51, in terms of code delay and Doppler frequency estimation errors is illustrated in Figure 9.

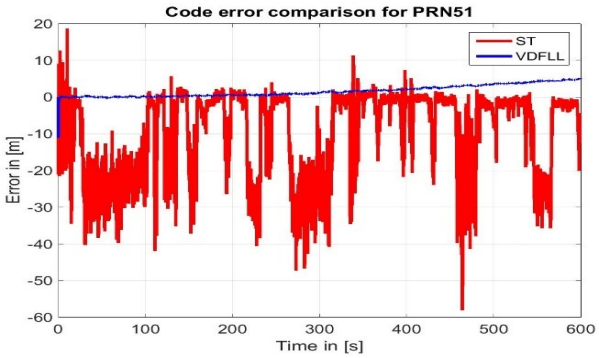

a)

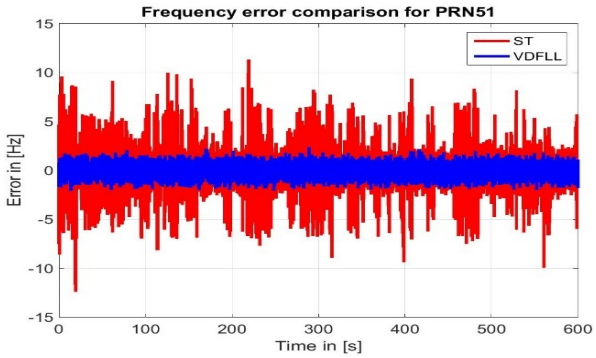

b)

Figure 9 – a) Code delay estimation error (in m); b) carrier frequency estimation error (in Hz) for the scalar tracking (in red) and VDFLL algorithm (in blue) of Galileo PRN 51 in NLOS condition.

Based on the multipath PDP profile of Galileo PRN51 in Figure 5 b), three major satellite blockages are observed in the first 100 s, after 300 s and at around the 375 s, with the last event representing the shortest LOS-to-NLOS transition but characterized by the highest power decrease. In the scalar tracking configuration, the NLOS satellite tracking process is interrupted after the lock detection test failure, which requires the start of the reacquisition process, as the case for Galileo PRN 51 in Figure 9 a).
A marked robustness of the vectorized architecture concerning the code and carrier tracking processes can be easily noticed. The likely reason for this behavior is linked to the VDFLL capability of correctly estimating the ionosphere residual error contribution as shown in Figure 8 a). It must be pointed out, that the code/carrier tracking estimation process in continuously carried on by the VDFLL architecture even for the NLOS satellites based on the mutual channel aiding.

The code delay and Doppler frequency estimation statistics in terms of their mean and RMS values for the scalar and vectorized architectures are summarized in **Erreur ! Référence non valide pour un signet.**.

Table 3 – Galileo PRN 51 channel error statistics comparison.

	Scalar + KF			VDFLL		
	E[]	RMS[]	95%	E[]	RMS[]	95%
Code error $[m]$	9.9	15.8	31.2	1.7	2.2	4.1
Freq. error $[Hz]$	~0	2.9	5.3	~0	2.1	4.2

The VDFLL superiority in the channel estimation is verified from the statistics illustrated in Table 3. Indeed, the VDFLL code delay estimations are nearly 8 times more precise w.r.t the scalar tracking operation mode of the Galileo PRN51 characterized by frequent NLOS signal reception. This represents an evident confirmation of the channel aiding characteristic of the VDFLL algorithm.

6 CONCLUSIONS AND FUTURE WORK

In this paper, a vector delay/frequency-locked loop (VDFLL) architecture for a dual constellation L1/E1 GPS/Galileo receiver in urban environment is proposed. The originality of this work resides in the implementation of a dual-constellation VDFLL algorithm that is capable of estimating the ionosphere residual error along with its evolution in time.

After the mathematical description of the EKF filter's prediction and observation model, a detailed performance comparison in the position and tracking domain between the scalar tracking + KF positioning and VDFLL configuration, both operating at the same 50 Hz rate, was assessed under simulated ionosphere and multipath reception conditions using the DLR urban channel model. The results for the dynamic scenario showed that contrary to the conventional tracking, the L1/E1 VDFLL loop is able to provide a stable positioning solution even with a reduced number of satellites in view and in harsh signal fading conditions. Moreover, neither signals loss of lock conditions, nor reacquisition process is performed by the vectorized loop under high user dynamics or signal fading conditions. The reason for this behavior is linked to the inter-channel aiding through the update process based on the forward position/velocity projection in the vectorized architecture.

Future work will proceed on three fronts. First, the detailed performance analysis concerning the position and tracking accuracy will be extended to the cascaded vectorized architecture including a L1/E1 EKF estimation block per tracked channel. Secondly, a vectorized PLL will be investigated in order to fully accomplish the positioning and tracking capability of vector tracking in signal-constrained environment. Last but not least, the ultra-tight coupling of the VDFLL architecture with a low-cost MEMS sensor will be implemented and tested in harsh urban conditions.

ACKNOWLEDGMENTS

This work was financially supported by EU FP7 Marie Curie Initial Training Network MULTI-POS (Multi-technology Positioning Professionals) under grant nr. 316528.

REFERENCES

[1] J. J. Spilker Jr., "Fundamentals of signal tracking theory," in *Global Positioning System: Theory and Applications, Volume 1, Chapter 7, ser. Progress in Astronautics and Aeronautics*, Washington DC, 1996.

[2] Pany T, Kaniuth R, Eissfeller B., "Deep Integration of Navigation Solution and Signal Processing" *Proc. ION-ITM-2005*, Long Beach, California, pp 1095 – 1102.

[3] Kaniuth R, Eissfeller B., "Deep Integration of Navigation Solution and Signal Processing" Proc. ION-ITM-2005, Long Beach, California, pp 1095 – 1102.

[4] Lashley, M., Bevly, D.M., Hung, J.Y., "A Valid Comparison of Vector and Scalar Tracking Loops," *Proceedings of IEEE/ION PLANS 2010*, Indian Wells, CA, May 2010, pp. 464-474.

[5] Petovello, M. G., & Lachapelle, G. (2006, September). Comparison of vector-based software receiver implementations with application to ultra-tight GPS/INS integration. In *Proceedings of ION GNSS* (Vol. 6).

[6] X. Tang, G. Falco, E. Falletti and L. Lo Presti, "Theoretical Analysis and Tuning Criteria of the Kalman Filter-based Tracking Loop", *GPS Solutions 2014*, DOI: 10.1007/s10291-014-0408-2

[7] DLR, "Implementation of the Land Mobile Satellite Channel Model - Software Usage." 2007.

[8] DLR, "Land Mobile Satellite Channel Model - Interface Control Document." 2008.

[9] Brown, R. G., & Hwang, P. Y. (1997). Introduction to random signals and applied Kalman filtering: with MATLAB exercises and solutions. *New York: Wiley, c1997.*

[10] P.D. Groves, *Principles of GNSS, inertial, and multisensor integrated navigation systems*, 2013

[11] ICAO, *MOPS for GPS/ABAS Airborne Equipment*, Apr. 2009.

[12] EUROCAE, *MOPS for Airborne Open Service Galileo Satellite Receiving Equipment*, 2010.

[13] Shytermeja, Enik, Garcia-Pena, Axel, Julien, Olivier, "Performance Evaluation of VDFLL Architecture for a Dual Constellation L1/E1 GNSS Receiver in Challenging Environments," *Proceedings of the 29th ION GNSS+ 2016*, Portland, Oregon, September 2016, pp. 404-416.

[14] Elliott D. Kaplan, Christopher J. Hegarty, "Understanding GPS: Principles and Application," 2nd edition, Artech House, 2006

[15] Betz, J.W. (2002), Binary Offset Carrier Modulations for Radionavigation, *Navigation: Journal of the Institute of Navigation*, Vol. 48, Number 4, pp. 227-246.